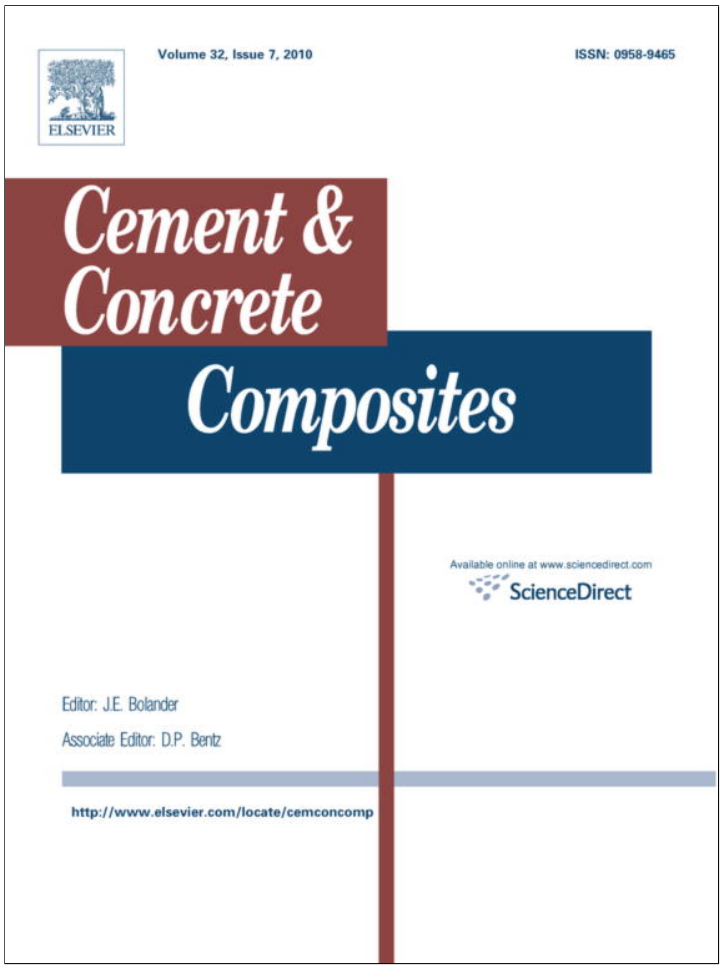

Cement & Concrete Composites 32 (2010) 532–543

Contents lists available at ScienceDirect

Cement & Concrete Composites

journal homepage: www.elsevier.com/locate/cemconcomp

# Strength of bolted moment connections in ferrocement construction

M.A. Mansur [a], K.L. Tan [b], A.E. Naaman [c,*]

[a] Faculty of Civil Engineering, Universiti Teknologi Malaysia (UTM), Johor, Malaysia
[b] Department of Civil Engineering, National University of Singapore, Kent Ridge, Singapore
[c] Department of Civil and Environmental Engineering, University of Michigan, Ann Arbor, Michigan, United States

ARTICLE INFO

*Article history:*
Received 13 November 2008
Received in revised form 15 April 2010
Accepted 15 April 2010
Available online 20 April 2010

*Keywords:*
Connections (bolted)
Composite materials
Ferrocement
Moment joints
Prefabricated panels
Strength
Tests

ABSTRACT

In continuation of an experimental investigation reported earlier by the authors on bolted moment joints in ferrocement construction, this study regards (1) further testing of ten such joints to broaden the range of the principal parameters – thickness of the connected ribs and location of bolts and (2) simple analytical modeling for design. Test results, as presented and discussed in this paper, indicate that the mode of failure of a joint depends on whether the applied moment is in the opening or closing mode. Under the closing mode, failure always occurs by shear punching of the bearing plates through the connected ribs. In contrast, failure in the opening mode occurs by bending failure of either the connected or the longitudinal rib. Based on observed failure modes, expressions have been derived for predicting the strength of such a joint. A comparison of theoretical predictions with present test results and those reported earlier shows good agreement.



## 1. Introduction

In recent years, ferrocement composites have made remarkable advances and gained considerable momentum not only in the utilization of advanced materials and special compositions, but also in various aspects of their manufacture. A number of technical documents are available in the literature summarizing these advances. They include a state-of-the-art report and a design guide by the American Concrete Institute [1,2], a ferrocement model code [3], a textbook [4], several symposia proceedings [5–11] and special conference reports [12–15]. Among notable advances, mechanized fabrication of reinforcement armature, employment of modern precast technology and use of bolted connections to assemble precast units can transform ferrocement, once regarded as a low-technology construction material, into a quality material of choice in many practical applications. Naaman [4], in a classic book on the subject, has provided a comprehensive illustration of what can be achieved with ferrocement.

Among the advanced technologies applied to ferrocement, the concept of connecting a thin-walled element by bolts opens up a whole new range of possibilities for exploring innovative applications embracing high-level industrialized construction techniques. One such application for the construction of a two-storey housing system [16,17] using precast channels and half-box panels is shown in Fig. 1. In this system, the bolted connections transmit a combination of moment, shear force and axial force between the panels, as shown for a typical module in Fig. 2. From the viewpoints of basic structural action, these connections may be classified as either "shear joints" or "moment joints". While investigations reported in the literature [18–22] on shear joints provide useful design guidelines, technical information on moment joints still remains very scarce [23,24], and insufficient to carry out a rational design.

The first investigation on bolted moment connection between ferrocement elements was reported by Hammoud and Naaman [23]. In their study, they used two L-shaped panels, connected back-to-back by bolts through one of the legs, as shown in Fig. 3a. Although test results have shown that the strength of such a joint can exceed the body strength of the panel, it does not truly represent the joint between the half-box panels shown in Fig. 2. As the introduction of the longitudinal ribs (see Fig. 3b) could vastly increase the strength and stiffness of the main body of the panels, a completely different type of response would be expected.

In an attempt to understand the behavior and strength of a realistic joint for the housing system conceived [17], the authors have conducted an experimental program on moment joints between two ferrocement half-box panels [25]. The joints were formed by assembling two almost full-scale size panels along the transverse ribs using two, symmetrically placed, bolts with square washer as can be seen in Fig. 3b. The main parameters considered were the thickness of the connected ribs and the horizontal and vertical

* Corresponding author.
*E-mail address:* naaman@umich.edu (A.E. Naaman).

0958-9465/$ - see front matter © 2010 Elsevier Ltd. All rights reserved.
doi:10.1016/j.cemconcomp.2010.04.001

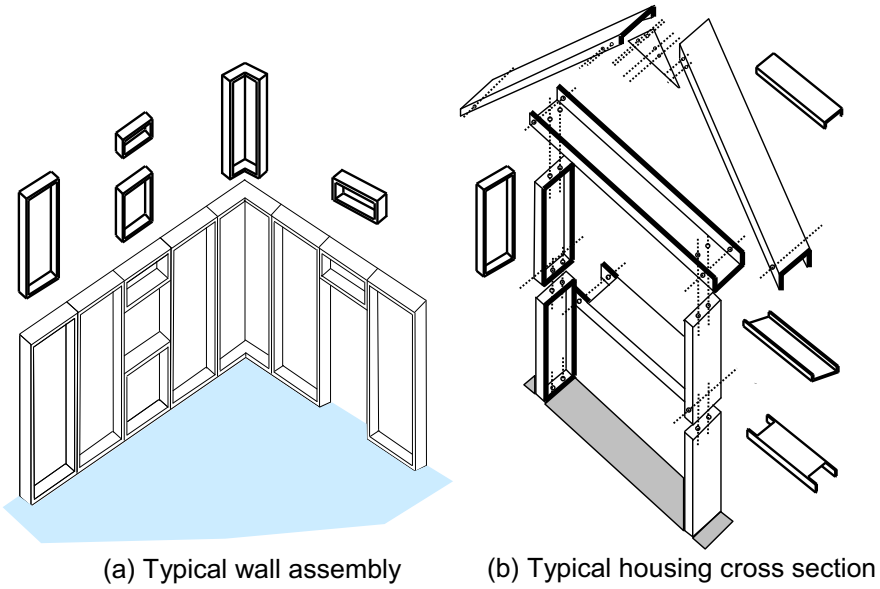


**Fig. 1.** Proposed housing system: prefabricated thin-wall panels are assembled by using bolted connections.

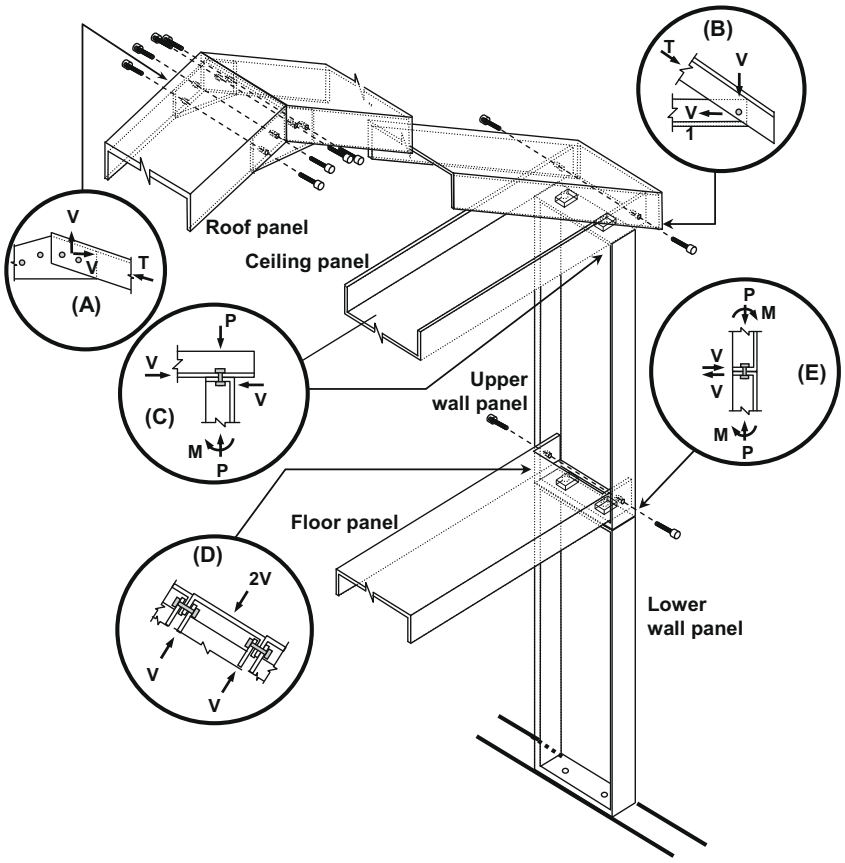


**Fig. 2.** Typical module of a panel assembly.

locations of the bolts (*X* and *Y* coordinates as shown later in Fig. 5). Test results have shown that for bending in the closing mode, failure occurs consistently by punching of the connected rib at bolt locations. In contrast, failure in the opening mode is dominated by bending. Depending on the location of the bolt, failure may take place either by transverse bending of the connected rib or vertical bending of the longitudinal rib at a section next to the joint. The latter mode of failure, which occurred for a bolt location closer to the longitudinal rib' is however frequently associated with splitting of the connected rib. It was concluded that the overall performance of the joint could be improved by shifting the bolts closer to the longitudinal ribs, increasing the distance between the bolts and

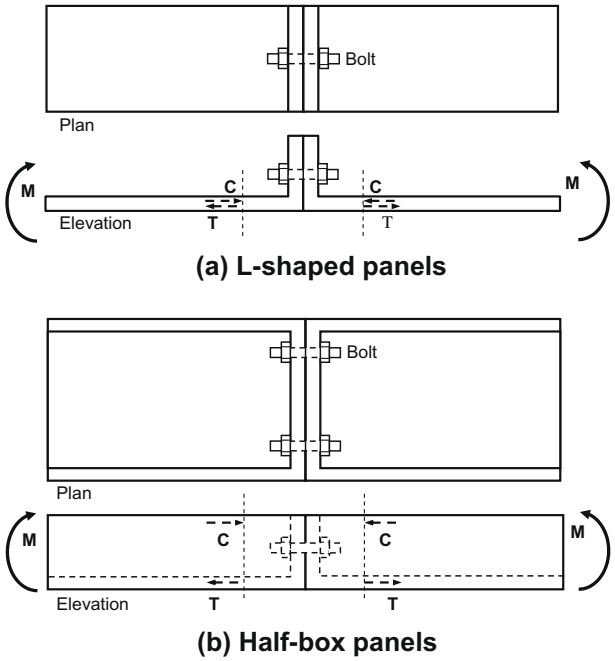


**Fig. 3.** Moment joints involving different types of panels tested in previous studies.

the compression zone, and increasing the thickness of the connected ribs. However, no attempt was made to develop analytical modeling to estimate the strength of such a joint.

The present investigation is undertaken to extend the study carried out earlier [25], explore additional parameters, and suggest a simple mechanistic model for predicting the strength of such a joint. It leads to a better understanding of the behavior and mechanisms of failure of bolted connections between thin-walled ferrocement structural elements and fills a knowledge gap in the current technical literature on the subject.

## 2. Experimental program

The half-box panels considered here have the same shape and dimensions as used in an earlier study [25]. Each panel was 1500 mm-long, 500 mm-wide with 150 mm-deep ribs as shown in Fig. 4a. The thickness of the rib in the long direction was fixed at 20 mm while that in the short direction was varied from 20 mm to 30 mm for different panels (see Table 1). The flat face of the panel was 15-mm thick. All panels were symmetrically reinforced across the thickness with a target clear cover of 3 mm on either face using the same amount and arrangement of reinforcement as shown in Fig. 4b and c, except for the connected (transverse) ribs in panels for joints designated C7–C10 and O7–O10 in Table 1. In these cases, the reinforcing mesh layers were lumped together at the outer face of the rib with a clear cover of 3 mm, as can be seen in Fig. 4d, because such an arrangement provide a better joint strength compared to the symmetrical arrangement [25]. A 6 mm diameter deformed wire was used along the outer end of the ribs to provide additional bending resistance. A small strip of fine wire mesh was wrapped around this wire to prevent it from bulging out of the panel. Bolt holes at appropriate locations were created during casting of the panels. The properties of reinforcement used are indicated in Fig. 4.

The joints were formed by assembling two panels back-to-back along the short (transverse) ribs using two, symmetrically placed (see Fig. 5), 12 mm-diameter high-strength steel bolts with 50 mm square washers. The washers were prepared from 10 mm-thick harden steel plates. The joints are designated by a number with a prefix O or C, indicating that the assembly was tested in opening (Fig. 5a) or closing mode (Fig. 5b), respectively. In all the joints, the bolts were located vertically at a maximum distance allowed by the panels from its compression face. This resulted in $Y = 105$ mm and $Y = 45$ mm for bending in the opening and closing modes, respectively (see Fig. 5c). Horizontally, they were located at a distance $X = 75$ mm from the outer face of the longitudinal rib for joints 6 and 7. The corresponding distance for the remaining joints was maintained at 50 mm, the closest value permitted by the panels. The values of the main test parameters, $X$, $Y$ and the thickness of the connected rib, $t_c$ for each joint are presented in Table 1.

The materials and the methods of fabrication and testing used in the present test program are identical to those employed in the earlier study [25]. In particular, the mortar matrix consisted of ordinary Portland cement and natural sand passing through US Sieve No. 16 (1.18 mm) in the ratio of l:2 by weight. In the mix, 15% by weight of cement was replaced by fly ash. The water-cement ratio used was 0.5 by weight for a target mortar strength of 50 MPa. Suitable admixtures with dosage conforming to manufactures' recommendations were added to improve workability and accelerate early development of strength. The joint assembly was simply supported over a span of 1.5 m with an overhang of 750 mm on either side and was tested under third-point loading, as shown in Fig. 6. As a result, the joint was subjected to a pure bending moment. Further details are presented elsewhere [25].

## 3. Test results and discussion

### 3.1. General behavior and modes of failure

In general, the behavior of joints tested in this program was very similar to that reported earlier [25]. But, because of locating the bolts closer to the longitudinal ribs, the two joining faces in the opening mode bending remained in full contact until failure. The increased amount of deformation is accommodated in the vertical cracks that develop in the longitudinal ribs right at the intersection with the transverse rib, irrespective of the bolt position used in this study. Failure occurred by gradual widening of this crack and subsequent development of splitting cracks in the connected rib (Fig. 7b).

In the earlier study, a different response was observed when the bolts were located far away from the longitudinal ribs. In those cases, the two joining faces remained in full contact only during the initial stages of loading. But upon further loading, these joint started to rotate, apparently hinging at the top (compression side) of the panel and separating the two faces. This separation appeared to be linear across the depth of the panel from a side view. However, a closer examination revealed that the separation did not remain uniform all along the joining faces. The central area, described approximately by a rectangle having a length equal to the distance between the outer edges of the washers and width equal to the distance between the compression side and extreme edge of the washer did, in fact, remain in close contact during the loading process. This implied that the portion of the connected rib between the bolt and the longitudinal rib was subjected to transverse bending which finally led to the failure. This can be clearly seen in Fig. 7a.

When the moment applied is in the closing mode, the joint opens up on the tension side approximately in a uniform manner across the entire width of the panel. Since the central part is held together by the bolts, increasing amount of rotation with an increase in the applied load results in gradual punching of the rib around the periphery of bolt washer, leading eventually to a clear punching shear failure (see Fig. 8). All closing joints, irrespective of rib thickness and bolt location, failed in this manner.

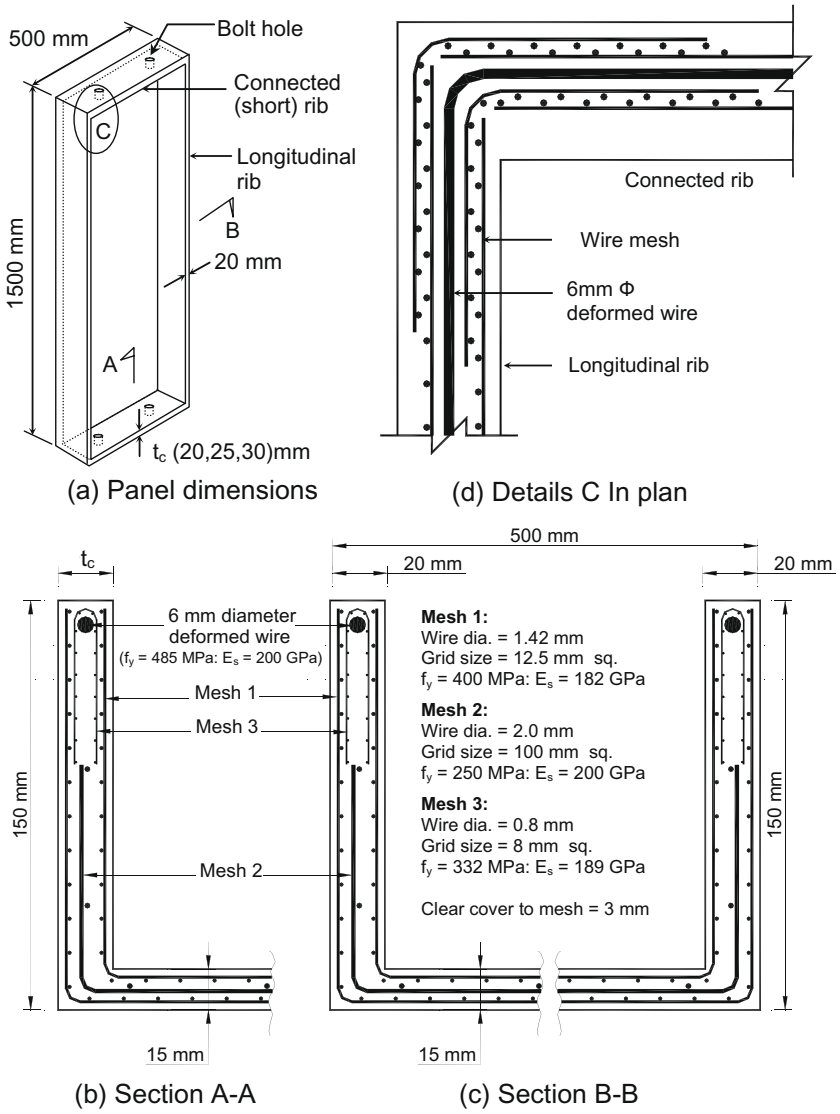


**Fig. 4.** Dimensions and reinforcement details of panels.

### 3.2. Moment–rotation response

The applied moment vs. rotation curves for the joints tested in the opening and closing modes are presented in Fig. 9a and b, respectively. In these figures, the results corresponding to $t_c$ = 20 mm and $X$ = 75 mm have been extracted from the previous study [25] to have a complete range of parameters. It may be observed that the shape of the curves is remarkably similar to the typical moment–curvature relationship exhibited by a reinforced concrete section. Each curve is characterized by three regimes – uncracked elastic regime followed by a cracked, but reasonably elastic response with a reduced slope. Final regime consists of a horizontal branch, similar to yielding, where the joint keeps rotating at approximately the same moment. However, the third regime is very short for the joints tested in closing mode bending. It may be recalled here that these joints failed by punching of bolt washers through one of the connected ribs. A sharp drop in the applied moment immediately after reaching the peak value is most likely the reflection of the brittle nature of punching shear failure. It may be interesting to note that for a particular bolt location, all joints reached the ultimate moment capacity at about the same rotation, irrespective of the thickness of the connected rib. Similar to the findings reported in the earlier study [25], it is found that most of the rotation took place at the joints and that the contribution of bending deformation of the panels to associated deflection was negligible.

### 3.3. Ultimate strength

The ultimate moment capacities attained by the joints may be noted in the moment–rotation curves of Fig. 9, and the corresponding numerical values are summarized in Table 1. It is observed that for a particular bolt location, an increase in thickness of the connected ribs increases the ultimate moment capacity of the joint, as anticipated. Similarly, for a given rib thickness, moving the bolts closer to the longitudinal rib dramatically improves the strength of the joint, but only for those tested in the opening mode bending. In the closing mode, the trend is however different. It may be recalled that these joints failed in punching shear. Moving the bolts closer to the longitudinal ribs may lead to a reduction in the punching shear perimeter and, consequently, a reduction in joint strength. This is what happened in the present case; joints with $X$ = 50 mm (Fig. 5) exhibited a smaller capacity than those with $X$ = 75 mm. The above observations regarding the effect of horizontal position

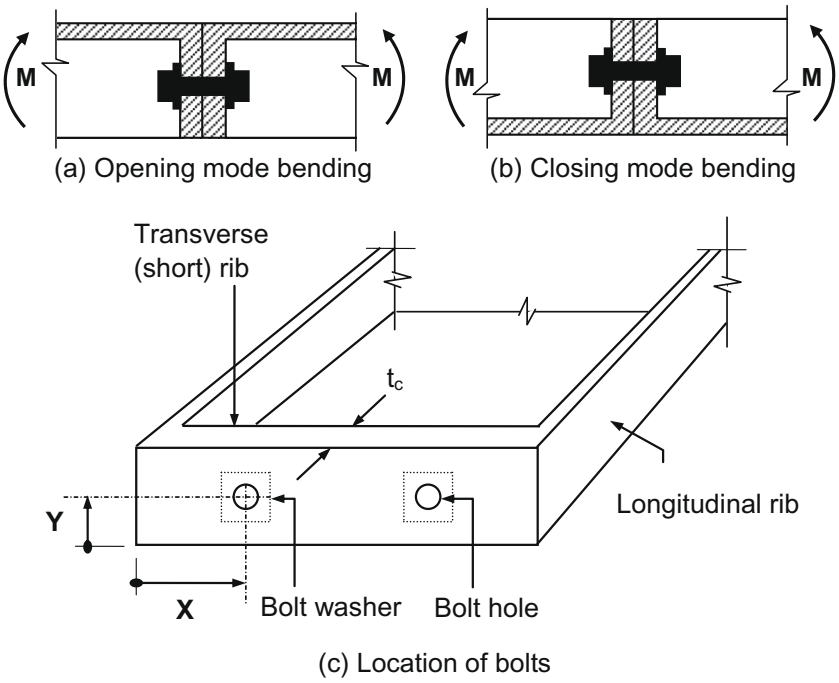


**Fig. 5.** Bending modes and test parameters.

**Table 1**
Test program and ultimate strength of joints.

| Mode of testing | Joint | Thickness of connected ribs, $t_c$ (mm) | Horizontal location of bolts, $X$[a] (mm) | Vertical location of bolts, $Y$[a] (mm) | Cylinder compressive strength of mortar, $f'_c$ (MPa) | Ultimate strength of joint, $M_{u,test}$ (kNm) | Ratio of joint strength to body strength (%) |
|---|---|---|---|---|---|---|---|
| Opening mode | O6 | 25 | 75 | 105 | 61.2 | 1.25 | 21.4 |
| | O7 | 30 | | | 61.2 | 2.25 | 38.5 |
| | O8 | 20 | 50 | | 61.1 | 1.80 | 30.9 |
| | O9 | 25 | | | 59.7 | 2.63 | 45.1 |
| | O10 | 30 | | | 54.1 | 4.09 | 70.1 |
| Closing mode | C6 | 25 | 75 | 45 | 61.2 | 2.55 | 36.4 |
| | C7 | 30 | | | 61.2 | 4.02 | 57.4 |
| | C8 | 20 | 50 | | 61.1 | 1.64 | 23.4 |
| | C9 | 25 | | | 59.7 | 3.30 | 47.2 |
| | C10 | 30 | | | 54.1 | 3.45 | 49.2 |

[a] See Fig. 5.

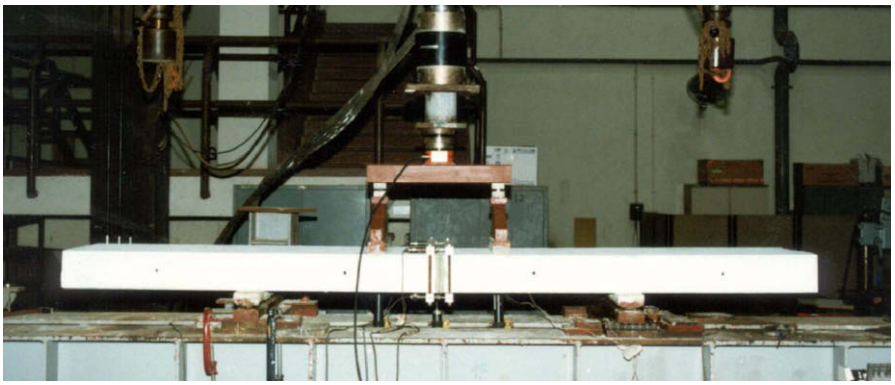

**Fig. 6.** Test setup.

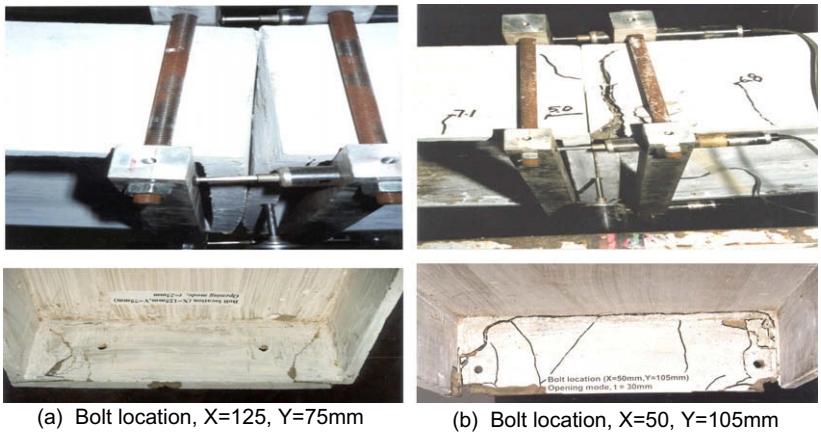


**Fig. 7.** Typical failure of joints in opening mode.

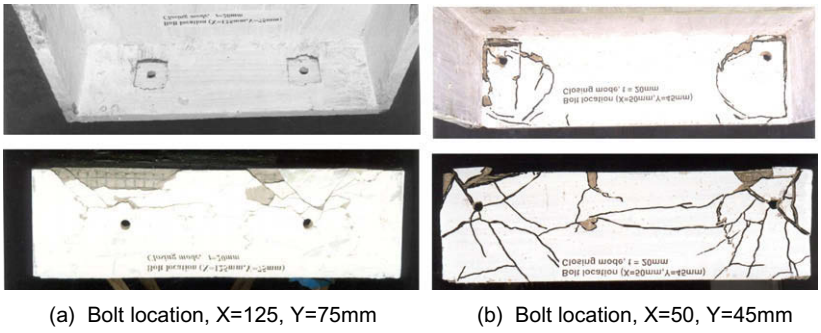


**Fig. 8.** Typical failure of joints in closing mode.

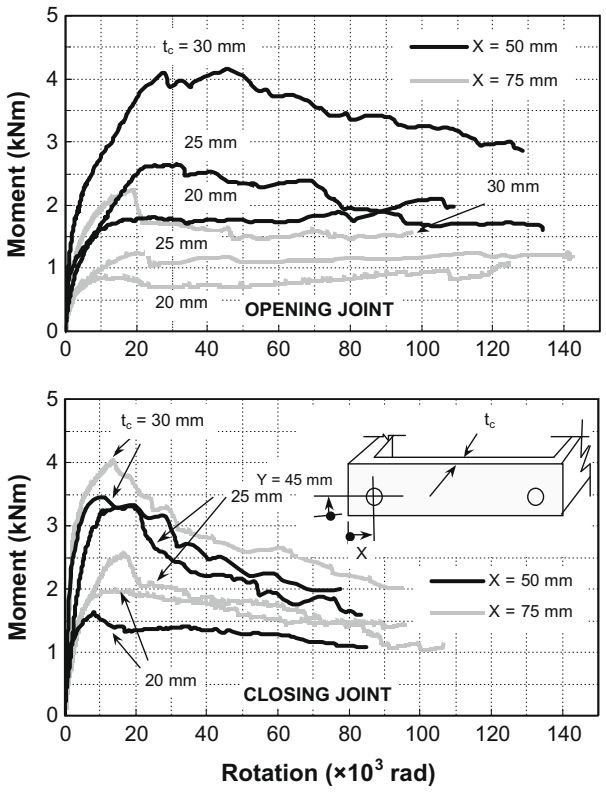


**Fig. 9.** Moment–rotation curves.

of the bolt, that is *X*, are in contrast with what was reported in the earlier study [25]. For the range of *X* used in that study, it was concluded that the strength of the joint remained practically unaffected if the bolts were shifted closer to the longitudinal ribs by keeping the same vertical position. However, the observations made in this study reveal that this conclusion is not valid for the whole range of this parameter. There appears to be an optimum bolt location to achieve the best performance in terms of both strength and stiffness of the joint, and this location is likely to correspond to the distance that does not lead to a reduction in punching shear perimeter.

## 4. Analysis for ultimate strength

From the tests conducted in the present program and those reported earlier, it is clear that for a suitably detailed moment joint, the mode of failure depends on the direction of moment applied to the joint. Accordingly, the joints are classified as either "opening joints" (*OJ*) or "closing joints" (*CJ*). For opening joints, failure may occur in two different modes depending on the horizontal location of the bolt. In the case of closing joints, however, failure always occurs by punching of the washer through the connected ribs, irrespective of bolt location. Based on these observed failure modes, equations are developed in the following section for predicting the strength of a joint.

### 4.1. Opening joint

For an opening joint, two modes of failure have been identified: *Mode 1* is due to transverse bending of the connecting (or transverse) rib, and *Mode 2* is due to bending of the longitudinal rib,

as shown in Fig. 7a and b, respectively. These are also schematically illustrated in Fig. 10.

*4.1.1. Analysis for Mode 1*

*Mode 1* failure (due to the transverse bending of the connecting rib) occurs when the bolt is located far away from the longitudinal rib. In such a case, the central portion of the connected (or connecting, or transverse) ribs between the two bolts remains locked, as was observed during the experiment. The forces developed in the longitudinal ribs due to the global flexural action, shown by dotted arrows, therefore tend to induce local bending of the free ends of the connected rib on either side. Failure occurs when the transverse bending capacity or the flexural shear capacity of the connected (transverse) rib is reached. Accordingly, this mode of failure is sub-classified as *Mode 1M* and *Mode 1V*, respectively.

For the purpose of analysis, it is assumed that the failure line is skewed and it traverses from the corner of the panel to the free edge of the connected rib via the edge of the washer at mid-depth, as shown in Fig. 10a. This line represents the critical section for *Mode 1M* failure. For *Mode 1V* failure, the critical section is assumed to be at distance $t_{cr}$ from the edge of the washer at mid-depth, as shown in Fig. 10c. The tensile stress resultant, *F*, in each longitudinal rib that arises from global action generates local bending in the connected rib. It is located at a distance, *d* from the extreme compression face, as shown. Therefore, referring to the free-body diagram of Fig. 10b and considering the moment equilibrium of the panel as a whole, we may express *F* in terms of the applied moment, $M_a$ as:

$$F = \frac{M_a}{2k_1 h} = \frac{M_a}{2\left(d - \frac{x}{2}\right)} \tag{1}$$

where $k_1 h$ is the lever arm between tensile and compressive stress resultants, *h* is the overall depth of panel, and *x* is the depth of compression stress block.

The transverse bending moment, $M_t$, generated by this force along the skewed failure (yield) line is given by

$$M_t = Fe \tag{2}$$

where *e* is the perpendicular distance of *F* from the failure line and is given by

$$e = d \sin \alpha \tag{3}$$

where $\alpha$ is the angle of the failure line with respect to the longitudinal rib.

Substituting the value of *e* from Eq. (3) into Eq. (2) and equating the resulting *F* with that in Eq. (1), we obtain

$$M_a = 2M_t \frac{\left(d - \frac{x}{2}\right)}{d \sin \alpha} \tag{4}$$

The bending moment capacity of the joint is obtained when $M_t$ reaches the transverse bending capacity of the connected rib along the failure line. Denoting this by $M_u$, the resulting joint capacity, $M_{OJ,1M}$ in *Mode 1M* failure is obtained as:

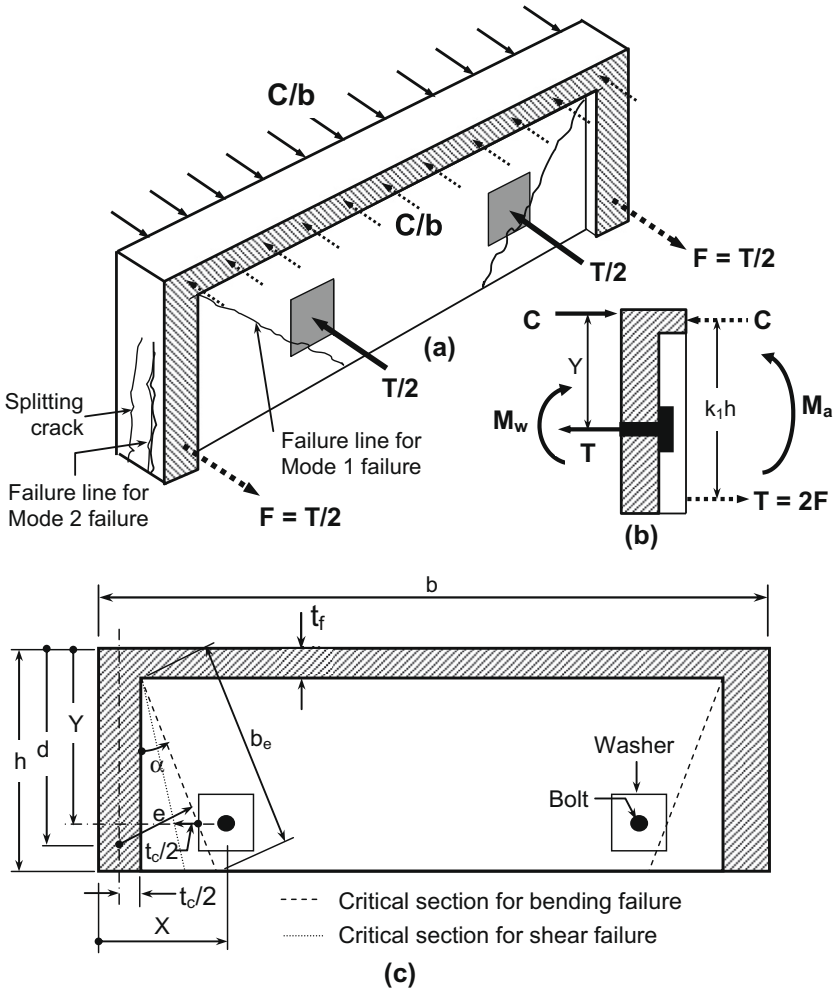


**Fig. 10.** Modeling of failure for an opening joint: (a) Three-dimensional view of the joint showing the forces developed, (b) Transverse view of the joint, and (c) Critical sections for bending and shear failure.

$$M_{OJ,1M} = 2M_u \frac{\left(d - \frac{x}{2}\right)}{d \sin \alpha} \quad (5)$$

While calculating $M_u$, the presence of any bar reinforcement and its direction should be taken into account.

For *Mode 1V* failure, the critical section is taken at a distance $t_c/2$ from the critical section for *Mode 1M* failure, as shown in Fig. 10c. If the equivalent ultimate shear stress is denoted as $v_u$, then the shear resistance, $V_u$, of the critical section is given by:

$$V_u = v_u \ell_{cs} t_c \quad (6)$$

where $\ell_{cs}$ is the length (or perimeter) of critical section for shear failure. It is noted that instead of the effective depth, the total depth (thickness) of the connected (or transverse) rib is used in Eq. (6), which is acceptable for ferrocement (Mansur and Ong [26]).

Setting, $V_u = F$, the moment capacity of the joint in *Mode 1V* failure is obtained from Eqs. (1) and (6) as:

$$M_{OJ,1V} = 2 v_u \ell_{cs} t_c \left(d - \frac{x}{2}\right) \quad (7)$$

In order to calculate $M_{OJ,1V}$, it is necessary to specify $v_u$. As recommended by Naaman [4], the value of $v_u = \frac{1}{3}\sqrt{f'_c}$ as specified in the ACI code [27] for conventional reinforced concrete is assumed in the present analysis for ferrocement. Thus, the final expression for $M_{OJ,1V}$ takes the following form:

$$M_{OJ,1V} = \frac{2}{3} \ell_{cs} t_c \left(d - \frac{x}{2}\right) \sqrt{f'_c} \quad (8)$$

*4.1.2. Analysis for Mode 2*

When the bolt is shifted closer to the longitudinal rib, the eccentricity, *e*, of the force *F* is reduced. As a result, failure occurs due to vertical bending of the longitudinal rib that arises from the global loading. However, as the joint between the longitudinal and the transverse ribs represents a location of potential weakness, failure always occurs at this section, and it is frequently associated with vertical splitting of the connected rib, as schematically shown in Fig. 10a.

If it is assumed that the connected rib remains intact and the failure is solely due to the bending of the longitudinal rib, then the capacity of the joint is identical to the bending resistance of the panel, $M_{u,panel}$. This means that sufficient embedment length for the reinforcement in the longitudinal ribs is available beyond the interface of the longitudinal and transverse ribs. However, the practical range of connected rib thickness employed in this study was insufficient to provide the full development length even for the fine wire mesh. Also, negotiating the reinforcement from the longitudinal ribs into the connected rib creates a highly complex stress situation in the corner region, similar to that which exists in a knee joint of a reinforced concrete frame. To mitigate the difficulty in mathematically formulating joint strength failure in this mode, a simple approach is used here by introducing a joint efficiency factor, $\eta$.

Looking at the results of joints O8–O10 in Table 1, where everything else was kept constant except for the thickness of the connected rib, $t_c$, it may be seen that the strength of the joint increases with an increase in $t_c$. This might be due to greater anchorage length furnished by thicker ribs. If the ratios of the experimental moment capacity, $M_{u,test}$ to the moment capacity of the panel, $M_{u,panel}$ are plotted against the connected rib thickness, a definite trend is observed (see Fig. 11). Using these test data, the joint efficiency factor, $\eta$, may be expressed in terms of the thickness of the connected rib, $t_c$ as:

$$\eta = 0.033 t_c - 0.38 \quad \leqslant 1.0 \quad (9)$$

where $t_c$ is in mm. Thus, the predicted joint capacity, $M_{OJ,2}$, for *Mode 2* failure of an opening joint may be taken as:

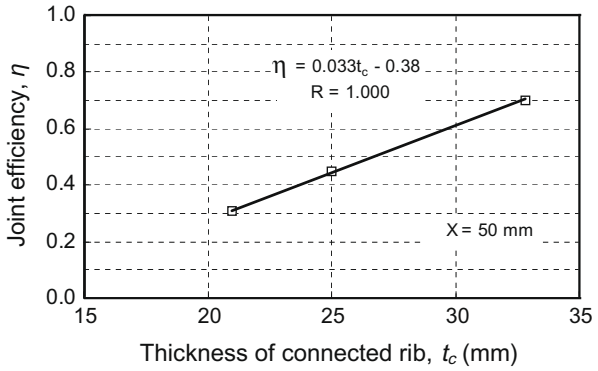


**Fig. 11.** Effect of connected rib thickness on joint efficiency.

$$M_{OJ,2} = (0.033 t_c - 0.38) M_{u,panel} \leqslant M_{u,panel} \quad (10)$$

*4.2. Closing joint*

As mentioned earlier, joints tested in the closing mode failed by punching of the washer irrespective of the location of the bolts. In order to calculate the forces involved in causing the punching shear failure, the free-body diagram of the connected rib is plotted in Fig. 12a. The applied stress resultants in the longitudinal direction (shown in dotted arrows) due to the global action produce the reactions as shown by the solid arrows. Referring to the side elevation shown in Fig. 12b, and considering equilibrium of forces in the longitudinal direction, it is noted that the washers are subjected to an axial load, *T*, as shown, the value of which is:

$$T = \frac{M_a}{k_1 h} \quad (11)$$

where $M_a$ is the applied moment at the joint and $(k_1 h)$ is the lever arm between the compressive stress resultant, *C* and tensile stress resultant, *T* due to global action.

Due to the differences in the lever arm between *C* and *T* for the two faces, the washer is subjected to a moment as well. Considering moment equilibrium about the center-line of the bolt, this moment, denoted as $M_w$, may be approximately represented by:

$$M_w = T(k_1 h - h + Y) \quad (12)$$

Thus, the washer is subjected to a combined moment and axial load, which becomes analogous to the case of punching shear around a column in flat plate structures due to an unbalanced moment. The maximum shear stress, $v_{max}$ around the critical perimeter may therefore be obtained as:

$$v_{\max} = \frac{V}{u_o t_c} + \frac{M_w c}{J_c} \quad (13)$$

where $V = T$, $u_o$ is the length of critical perimeter for punching shear failure, measured at a distance $t_c/2$ from the face of the washer, *c* is the distance of the critical perimeter from the center of the washer and $J_c$ is the polar moment of inertia for the critical section.

The capacity, $M_{CJ}$, of a closing joint is attained when $v_{max}$ reaches the ultimate shear stress, $v_u$. According to the ACI guide [2], and as recommended by Naaman [1], the strength under punching shear may be taken as twice that for flexural shear. Using this value of $v_u$ for $v_{max}$ in Eq. (13), substituting the values of $T$ (=$V$) and $M_w$ from Eqs. (11) and (12), respectively, and replacing $M_a$ by the joint capacity, $M_{CJ}$, we obtain:

$$M_{CJ} = \frac{2\left(\frac{1}{3}\sqrt{f'_c}\right)}{\frac{1}{k_1 h u_o t_c} + \frac{(k_1 h - h + Y)c}{k_1 h J_c}} \quad \leqslant M_{u,panel} \quad (14)$$

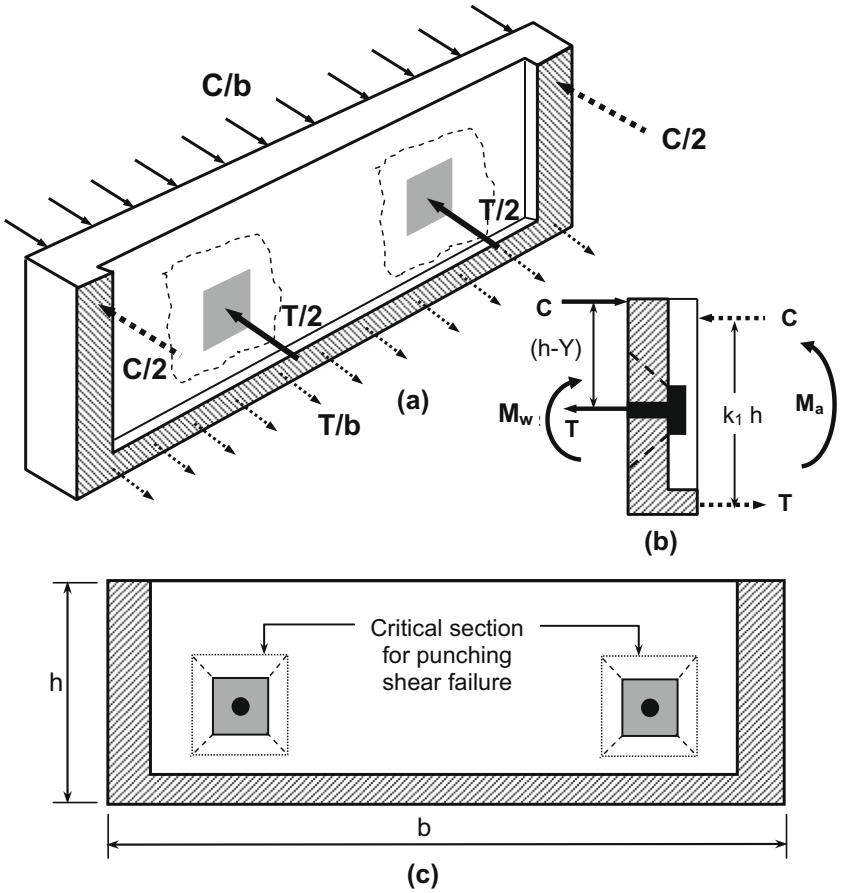


**Fig. 12.** Modeling of closing joint failure: (a) Three-dimensional view of joint showing the forces developed, (b) Transverse view of the joint, and (c) Critical section for punching shear failure.

It is clear that strength of the joint should be less than or at most equal to the panel strength, $M_{u,panel}$.

As the area of concrete available to develop the compressive stress resultant, $C$, due to global action is provided only by the longitudinal rib, the value of $k_1$ to be used in Eq. (14) should be smaller than that assumed for rapid assessment of the moment capacity of a reinforced concrete rectangular section. Unless assessed accurately, a value of 0.8 for $k_1$ is suggested as an approximation.

The above analysis applies when the failure surface in punching does not intercept either the longitudinal rib or the flat face of the panel. For example, when the bolt location is shifted vertically close to the face of panel, the critical section for punching shear failure will intercept the face, as shown in Fig. 13. The reinforcement in the flat face of the panel will then be subjected to direct tension, thus resulting in a reduction in the shear to be carried by the concrete. In such a case, assuming that the reinforcement has yielded, $V$ in Eq. (13) is given by:

$$V = T - T_f \tag{15}$$

where $T_f$ is the tensile force generated by the reinforcement in the flat face of the panel through the failure surface.

Similarly, the moment acting on the washer is:

$$M_w = T(k_1 h - h + Y) - T_f\left(\frac{w}{2} + \frac{t_f}{2} + s\right) \tag{16}$$

where $w$ = width of washer, $t_f$ = thickness of flange (flat face); $s$ = clearance between the flat face and the nearest edge of washer.

Eq. (14) then takes the following form:

$$M_{CJ} = \frac{2\left(\frac{1}{3}\sqrt{f'_c}\right) + \frac{T_f}{u_o t_c} + \frac{T_f(w/2 + t_f/2 + s)c}{J_c}}{\frac{1}{k_1 h u_o t_c} + \frac{(k_1 h - h + Y)c}{k_1 h J_c}} \leqslant M_{u,panel} \tag{17}$$

A closer examination of the details presented in Table 1 reveals that the bolt locations for joints designated C5–C10 were sufficiently close to the flat face for Eq. (17) to be applicable.

Similarly, interference of the failure surface by the longitudinal ribs as well would generate a more complex stress situation. However, for the joint details employed in this study, the bolts were located sufficiently away from the longitudinal rib to bypass its interference.

### 4.3. Comparison with test data

The ultimate strengths of all the joints tested in this program are calculated using the analytical expressions presented above. For each joint in the opening mode, all the three failure modes, that is, *Mode1M*, *Mode 1V* and *Mode 2*, were considered irrespective of what was observed in the experiment. The smallest of the three values is taken as the predicted ultimate strength and the corresponding mode as the predicted mode of failure. All joints in the closing mode are assumed to have failed in punching shear.

The results of these analyses are presented and compared with the corresponding test values in Tables 2 and 3 for opening and closing modes, respectively. It may be seen that the analyses presented herein correctly predicts the mode of failure, except for the *Mode 1V* failure. The ultimate strength and the effects of various test parameters are also predicted with a reasonable degree

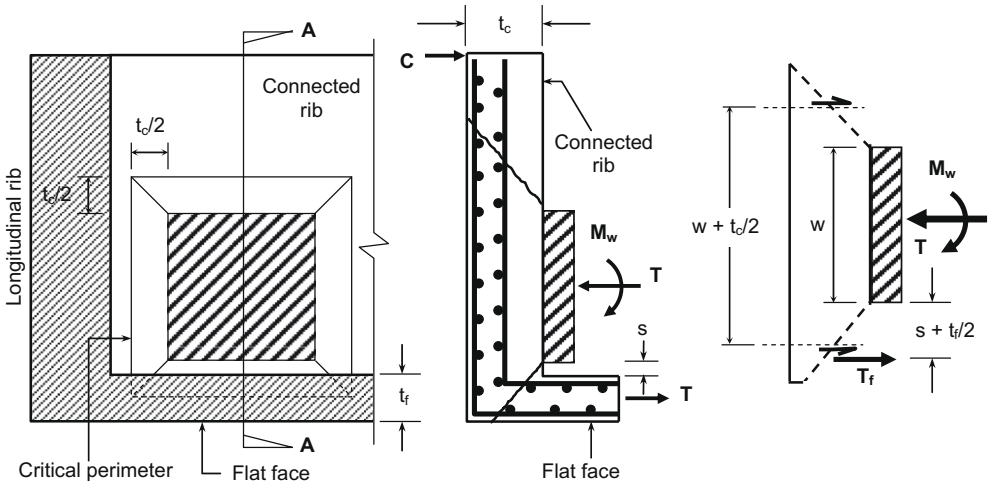


**Fig. 13.** Modifications when the failure surface encroaches on the flat face.

**Table 2**
Test results and comparison with theoretical predictions for opening joint.

| Source | Joint | Panel capacity, $M_{u,panel}$ (kNm) | Test | | Calculated moment capacity | | | Predicted | | $\frac{M_{u,test}}{M_{u,calc}}$ |
|---|---|---|---|---|---|---|---|---|---|---|
| | | | Ultimate strength of joint, $M_{u,\ test}$ (kNm) | Mode of failure | Mode 1 M, $M_{OJ,1M}$ (kNm) | Mode 1 V, $M_{OJ,1V}$ (kNm) | Mode 2, $M_{O2}$ (kNm) | Ultimate strength of joint $M_{u,calc.}$ | Mode of failure | |
| Mansur et al.[25] | O1 | 5.83 | 0.72 | 1 M | 0.51 | 2.41 | 1.52 | 0.51 | 1 M | 1.41 |
| | O2 | 5.78 | 0.72 | | 0.68 | 2.75 | 2.57 | 0.68 | | 1.06 |
| | O3 | 5.83 | 1.15 | | 0.87 | 3.59 | 3.67 | 0.87 | | 1.31 |
| | O4 | 5.82 | 0.69 | | 0.63 | 1.63 | 1.52 | 0.63 | | 1.09 |
| | O5 | 5.80 | 0.87 | 1 V | 0.83 | 1.50 | 1.49 | 0.83 | | 1.04 |
| Present study | O6 | 5.86 | 1.25 | | 1.39 | 2.15 | 2.61 | 1.39 | | 0.90 |
| | O7 | 5.86 | 2.25 | | 2.06 | 2.70 | 3.86 | 2.06 | | 1.09 |
| | O8 | 5.86 | 1.80 | 2 | N.A. | | 1.83 | 1.83 | 2 | 0.98 |
| | O9 | 5.86 | 2.63 | | | | 2.61 | 2.61 | | 1.01 |
| | O10 | 5.82 | 4.09 | | | | 4.09 | 4.09 | | 1.00 |
| | | | | | Average | | | | | 1.09 |
| | | | | | S.D. | | | | | 0.157 |

**Table 3**
Test results and comparison with theoretical predictions for closing joint.

| Source | Joint | Ultimate strength of joint (kNm) | | $\frac{M_{u,test}}{M_{u,calc}}$ |
|---|---|---|---|---|
| | | Test $M_{u,test}$ | Predicted $M_{u,calc}$ | |
| Mansur et al.[25] | C1 | 1.57 | 1.10 | 1.41 |
| | C2 | 1.82 | 1.54 | 1.18 |
| | C3 | 2.24 | 2.22 | 1.01 |
| | C4 | 1.55 | 1.14 | 1.36 |
| | C5 | 1.93 | 1.69 | 1.14 |
| Present study | C6 | 2.55 | 2.11 | 1.21 |
| | C7 | 4.02 | 2.88 | 1.40 |
| | C8 | 1.64 | 1.77 | 0.92 |
| | C9 | 3.30 | 2.42 | 1.37 |
| | C10 | 3.45 | 2.74 | 1.26 |
| | Average | | | 1.22 |
| | S.D. | | | 0.167 |

of accuracy. For the ten joints tested in opening mode, the ratio of experimental to predicted joint strengths $M_{u,test}/M_{u,calc.}$ ranges from 0.98 to 1.41, with an average of 1.09 and standard deviation of 0.16. In the closing mode, the ratio of $M_{u,test}/M_{u,calc}$ ranges from 0.92 to 1.41, the average and standard deviation being 1.22 and 0.17, respectively.

### 4.4. Parametric investigation

Based on the equations developed, computer analyses have been carried out to study the influence of various parameters on ultimate strength and modes of failure of the joints. In the analysis, it was assumed that the overall panel dimensions remain the same as those used in this study and that mortar strength, $f'_c$, is fixed at 50 MPa. It is further assumed that the section contains fine wire mesh with a grid size of 12.5 × 12.5 mm and wire diameter of 1.42 mm, and one rebar near the open end of each longitudinal ribs. The joints were analyzed by varying the layers of wire mesh (two and three), the horizontal location of bolt, $X$ (from 60 to 200 mm), vertical location of bolt, $Y$ (from 75 to 105 mm for opening joint and from 45 to 75 mm for closing joint), thickness of connected rib, $t_c$ (from 20 to 50 mm). Using these wide ranges of geometric and reinforcement parameters, predicted ultimate moments and failure modes were generated for both opening and closing joints. For brevity, only the important observations made from these analyses are summarized without any elaboration.

For an opening joint with fixed bolt location, strength predicted for each mode of failure increases as the thickness of the connected rib is increased. As the bolt is moved away from the longitudinal rib, keeping the vertical position fixed, strength predicted for *Mode 1M* failure first decreases reaching a minimum value. Further increase in $X/b$, where $b$ is the width of the panel, leads to an increase in the moment capacity of the joint. In contrast, the moment capacity for *Mode 1V* increases as the $X/b$ is increased. For *Mode 2*, however, it remains at a fixed value irrespective of the horizontal location of bolt. Thus *Mode 1M* is the predominant mode of failure, giving the smallest value for nearly the whole range of bolt

position. However, either *Mode 1V* or *Mode 2* governs the failure only when the bolt is located very close to the longitudinal rib, and such a position gives the maximum strength of the joint.

For a particular of *X/b*, a change in the vertical position of the bolt has practically no influence on the predicted strength for *Modes 1V* and *Mode 2*. However, an increase in the distance between the bolt location and the compression side of the panel, that is, an increase in the value of *Y/h* leads to an increase in the moment capacity for *Mode 1M* failure, and this mode usually governs the failure.

Other than the bolt location, the thickness of the connected (or transverse) rib plays an important role in enhancing the joint capacity. For a particular bolt location, an increase in the thickness of the connected ribs dramatically improves the joint capacity. Further enhancement in joint strength may be accomplished by increasing the amount of reinforcement in the connected ribs and lumping it near its outer face.

Thus, the strength or efficiency of an opening joint may be improved by increasing the thickness of the connected rib while proportionately increasing its reinforcement, and locating the bolt closer to the longitudinal rib utilizing the maximum distance available from the compression side of the panel.

In closing mode bending, failure always occurs by punching of the washer through one of the connected ribs. For this type of failure, the effects of the amount of reinforcement in the rib and horizontal location of the bolt are found to be insignificant. Thus, the thickness of the connected ribs and the vertical position of the bolts are the two major parameters affecting the strength of the joint. It has been found that for smaller values of *Y/h*, an increase in rib thickness may result in joint strength surpassing the bending capacity of the panel itself, thus resulting in the most efficient joint.

## 5. Summary and concluding remarks

The results of an experimental investigation conducted on 10 moment resisting joints in full-scale ferrocement half-box panels are reported. The connectors consisted of only two, symmetrically placed, steel bolts. The main parameters considered were the thickness of the ribs and the horizontal and vertical locations of the bolts. Test results indicate that an increase in the thickness of the connected lateral ribs and/or the distance between the bolts and the compression face of the ribs increases the ultimate resistance of the joint. Under the closing mode bending, failure occurred by punching shear of the bearing plates through the connected ribs, while under opening mode failure occurred in bending in either the connected rib or the longitudinal rib of the panel.

Based on the observed modes of failure analytical expressions were developed to predict the ultimate strength of a joint under either opening or closing mode bending. Analytical predictions were found to be in reasonably good agreement with the experimental test results generated in this study; they are recommended to be used as simple tools for design.

Using these expressions, a parametric study was carried out to further identify the main parameters affecting the joint capacity. It helped ascertain that the thickness of the connecting rib (that is, the transverse rib connecting the two longitudinal ribs of the panel) and the location of the bolts are the key parameters, assuming bolt strength is sufficient. Thus, for an efficient joint, the bolts need to be placed closer to the longitudinal ribs with a maximum shear section distance touching the compression side of the panel. The joint capacity is further enhanced by increasing the amount of longitudinal reinforcement in the connected rib and placing them on the outer face of the panel.

It is hoped that this study will not only advance the state of knowledge about ferrocement construction but also helps in the development of similar information on textile reinforced concrete such as for instance described in Ref. [28].

## Acknowledgements

The work reported in this paper is supported by Research Grant, R-264-000-016-112 with funds given by the National University of Singapore under a joint research program with the University of Michigan at Ann Arbor, USA. The reinforcement required for the project was partly donated by BRC Asia Ltd. The authors gratefully acknowledge these supports.

## References

[1] ACI Committee 549 (1997). State-of-the-art report on ferrocement. Concr Int 1982; 4(8): 13–38 [Reinstated as ACI 549-R97, in *Manual of Concrete Practice*, American Concrete Institute, Farmington Hills, Michigan, 26 p].
[2] ACI Committee 549, (1988, ...). Guide for the design, construction and repair of ferrocement. ACI 549.1R-88, ACI Struct J 1988: 325–51 [Also reinstated as 549.1R-93 and published in *ACI Manual of Concrete Practice*, American Concrete Institute, Farmington Hills, Michigan, 27 p].
[3] Ferrocement Model Code (2001) by IFS Committee 10-01. International Ferrocement Society, Asian Institute of Technology, Bangkok, Thailand, 95 p.
[4] Naaman AE. Ferrocement and laminated cementitious composites. Michigan (USA): Techno Press; 2000.
[5] Robles-Austriaco L, Pama RP, Sashi Kumar K, Mehta EG, editors. Proceedings of the second international symposium on ferrocement. Asian Institute of Technology, Bangkok, Thailand, International Ferrocement Information Center; 1985. 773 p.
[6] Wainshtok Rivas H, editor. Proceedings of the fourth international symposium on ferrocement. La Havana, Cuba; CETA, La Havana, Cuba; 1991.
[7] Nedwell PJ, Swamy RN, editors. Ferrocement: proceedings of the fifth international symposium. London: Manchester, E & FN Spon; 1994. p. 508.
[8] Naaman AE, editor. Ferrocement 6: Lambot Symposium. In: Proceedings of the Sixth International Symposium on Ferrocement, University of Michigan, Ann Arbor; 1998. 699 p.
[9] Mansur MA, Ong KCG, editors. Ferro-7: Proceedings of the seventh international symposium on ferrocement and thin reinforced cement composites. National University of Singapore; 2001. 558 p.
[10] Nimityongskul P, Naaman AE, Bolander JE, Jaturapitakkul C, Sujirovakul C, Sayamipuk S, editors. Ferrocement and Thin Reinforced Cement Composites. In: Proceedings of international conference and NSF workshop, FERRO-8, Bangkok, Thailand. International Ferrocement Society, Asian Institute of Technology, Thailand; 2006. 645 p. (ISBN/ISSN: 974-93905-1-X).
[11] Djausal A, Alami F, Naaman AE, Co-editors. Ferrocement and thin reinforced cement composites: green technology for housing and infrastructure construction. In: Proceedings of ferrocement 9, The University of Lampung, Bandar Lampung, Indonesia; 2009. 506 p. ISBN: 978-979-1165-93-8.
[12] ACI Committee 549. Report on Thin Reinforced Cementitious Products. 549.2R-04, American Concrete Institute, Farmington Hills, Michigan; 2004.
[13] Balaguru P, editor. Thin reinforced concrete products and systems. SP-146, American Concrete Institute, Farmington Hills, Michigan; 1994. 106 p.
[14] Daniel JI, Shah SP, editors. Thin-section fiber reinforced concrete and ferrocement. SP-124, American Concrete Institute, Detroit, Michigan; 1990. 448 p.
[15] Dubey A, editor. Thin reinforced cement-based products and construction systems. American Concrete Institute, Special Publication SP-224, Farmington Hills, Michigan; 2004.
[16] Naaman AE. Ferrocement housing: toward integrated high technology solutions. J Ferrocement 1989;19(2):141–9.
[17] Naaman AE, Hammoud H. Ferrocement prefabricated housing: the next generation. J Ferrocement 1992;22(1):35–47.
[18] Abdullah, Mansur MA. An investigation into the behavior and strength of bolted connections in ferrocement. J Ferrocement V 1995;25(3): 207–19.
[19] Hammoud H, Naaman AE. Ferrocement bolted shear joints: failure modes and strength prediction. J Cem Concr Compos 1998;20:13–29.
[20] Hammoud H, Naaman AE. Ferrocement bolted shear joints: finite element analysis and stress distribution. J Ferrocement V 2000;30(1):31–43.
[21] Krishnamoorty TS, Parameswaran VS, Neelamegam M, Balasubramaniam K. Investigation of precast ferrocement planks connected by steel bolts. *ACI Special Publication*, SP-124; 1990. p. 389–403.
[22] Mansur MA, Tan KL, Naaman AE, Paramasivam P. Bolt bearing strength of thin-walled ferrocement. ACI Struct J V 2001;98(4):563–71.
[23] Hammoud H, Naaman AE. Behavior of ferrocement moment resisting joints. Thin Reinforced Concrete Products and Systems. *ACI Special Publication*, SP-146; 1993. p. 111–130.

[24] Murali DK. Use of precast concrete walls and slab with bolted joints for buildings. Indian Concr J V 1997;71(2):73–7.
[25] Mansur MA, Tan KL, Naaman AE, Paramasivam P. Behavior of moment connections between ferrocement half-box panels. J Ferrocement V 1998;28(3):221–32.
[26] Mansur MA, Ong KCG. Shear strength of ferrocement I-beams. ACI Struct J Am Concr Inst V 1991;88(4):458–64.
[27] ACI Committee 318. Building Code Requirements for Structural Concrete (ACI 318-2002) and Commentary (ACI318RM-2002). American Concrete Institute, Farmington Hills, Michigan; 2002. 443 p.
[28] Dilthey U, Schleser M, Feldmann M, Pak D, Geßle A. Investigation of punctiform, plane and hybrid joints of textile-reinforced concrete parts. Cem Concr Compos 2008;30(2):82–7.